ACS APPLIED MATERIALS & INTERFACES

Research Article

www.acsami.org

Electrospun Bio-Nanocomposite Scaffolds for Bone Tissue Engineering by Cellulose Nanocrystals Reinforcing Maleic Anhydride Grafted PLA

Chengjun Zhou,[†] Qingfeng Shi,[†,‡] Weihong Guo,[‡] Lekeith Terrell,[§] Ammar T. Qureshi,[§] Daniel J. Hayes,[§] and Qinglin Wu*[,†,‡]

[†]School of Renewable Natural Resources, Louisiana State University Agricultural Center, Baton Rouge, Louisiana 70803, United States

[‡]School of Material Science and Engineering, East China University of Science and Technology, Shanghai 200237, China

[§]Department of Agricultural and Biological Engineering, Louisiana State University Agricultural Center, Baton Rouge, Louisiana 70803, United States

Supporting Information

ABSTRACT: Electrospun fibrous bio-nanocomposite scaffolds reinforced with cellulose nanocrystals (CNCs) were fabricated by using maleic anhydride (MAH) grafted poly(lactic acid) (PLA) as matrix with improved interfacial adhesion between the two components. Morphological, thermal, mechanical, and in vitro degradation properties as well as basic cytocompatibility using human adult adipose derived mesenchymal stem cells (hASCs) of MAH grafted PLA/CNC (i.e., MPLA/CNC) scaffolds were characterized. Morphological investigation indicated that the diameter and polydispersity of electrospun MPLA/CNC nanofibers were reduced with the increased CNC content. The addition of CNCs improved both the thermal stability and mechanical properties of MPLA/CNC composites. The MPLA/CNC scaffolds at the 5 wt % CNC loading level showed not only superior tensile strength (more than 10 MPa), but also improved stability during in vitro degradation compared with the MPLA and PLA/CNC counterparts. Moreover, the fibrous MPLA/CNC composite scaffolds were non-toxic to hASCs and capable of supporting cell proliferation. This study demonstrates that fibrous MPLA/CNC bio-nanocomposite scaffolds are biodegradable, cytocompatible, and possess useful mechanical properties for bone tissue engineering.

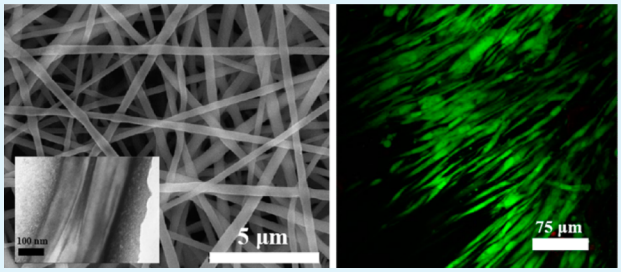

KEYWORDS: *electrospinning, cellulose nanocrystals (CNCs), nanocomposites, modification, poly(lactic acid), scaffolds*

INTRODUCTION

As one of the most promising nano-reinforcements for composites, cellulose nanocrystals (CNCs) have attracted considerable attention because of their unique features such as nano-scale dimensions, excellent mechanical properties, ease of chemical modification, high aspect ratio, low density, low energy consumption, inherent renewability, biodegradability, and biocompatibility.[1−3] Recently, one of the most exciting developments in processing CNCs reinforced composites has been the use of the electrospinning technique to generate continuous one-dimensional fibers with diameters ranging from several micrometers to less than 100 nm.[4] Because CNCs can be aligned under high electrostatic fields,[5] the electrospinning process facilitates the orientation of CNCs along the fiber axis, endowing electrospun nanocomposite fibers with significantly enhanced axial strength.[6,7]

Poly(lactic acid)s (PLAs) are biodegradable thermoplastic polyesters derived from renewable resources such as corn, wheat, and potato. PLA has been extensively investigated over the last several decades especially for use in the biomedical and tissue engineering fields because of its bioresorbable and biocompatible properties in living organisms, including the human body.[8,9] PLA is easily processed and has flexible mechanical strength, specific biological properties, and controllable degradation rates allowing it to overcome the limitations of inherent brittleness and difficulty for processing of traditionally bioactive/bioabsorbable ceramics for the scaffolds in bone and cartilage generation.[10]

Porous PLA-based scaffolds can be fabricated by a number of technologies including solvent casting, particulate leaching, membrane lamination, melt molding, and precise extrusion.[11,12] Several interesting studies have also demonstrated that PLA can be successfully processed to ultrafine fibrillar tissue scaffolds with highly porous 3D structures by the electrospinning technique, closely mimicking the natural extracellular matrix (ECM).[13,14] However, some limitations, including poor

Received: February 6, 2013
Accepted: April 1, 2013
Published: April 1, 2013

 © 2013 American Chemical Society

mechanical properties and low hydrophilicity of electrospun PLA scaffolds, limit its application in biomedical fields. Incorporating small quantities of nano-fillers (such as hydroxyapatite[15] and bioactive glass[16]) is a facile method to improve the properties of PLA scaffolds. Recently, bio-nanocomposite scaffolds made from CNCs and PLA were found to have both improved mechanical properties and controllable biodegradation.[17−20] However, interfacial fracture strength between PLA and CNCs is low as non-polar PLA and natural carbohydrate polymers are thermodynamically immiscible, resulting in a decrease in mechanical properties of PLA/CNC bio-nanocomposite scaffolds at high loading levels of CNCs. Surface modifications of PLA or CNCs are potential strategies to address this problem. Zoppe et al.[21] carried out chemical grafting with low-molecular-weight poly(ε-caprolactone) (PCL) diol onto the surface of CNCs in an attempt to improve the interfacial adhesion between CNCs and PCL matrix in electrospun nanocomposite scaffolds. However, it was found that the grafted CNCs had a negative effect on mechanical properties of nonwoven webs because the addition of modified CNCs induced the formation of heterogeneous morphologies (including nanofibrillar and annealed structures) and weakened the adhesion and stress transfer within the nanofibers.

Our approach in this study was to perform the surface modification of PLA with maleic anhydride (MAH) to yield better interaction between PLA and CNCs. Grafting with MAH can not only efficiently increase surface polarity of PLA and its compatibility with fillers by forming stronger hydrogen bonds between two phases,[22] but also improve the hydrophilicity of the nanocomposite scaffolds. Fibrous bio-nanocomposite scaffolds consisting of CNCs and MAH grafted PLA (MPLA) were fabricated using an electrospinning technique at room temperature. Morphological, thermal, mechanical, and in vitro degradation properties of nanocomposite scaffolds were characterized. Comparative cytocompatibility of nanocomposite scaffolds cultured on ungrafted and MAH grafted PLA were also investigated with human adult adipose derived mesenchymal stem cells (hASCs) for the model application in bone regeneration. hASCs have been used as a cell source for bone regeneration because of its osteogenesis.[23] The objective of the study was to develop a fully bio-based nanocomposite scaffolds material using modified PLA reinforced with CNCs and explore its potential application in bone tissue engineering.

EXPERIMENTAL SECTION

Materials. Cotton-based CNCs, with diameters varying from about 7 to 13 nm and lengths in the range of 80 to 140 nm, were fabricated using 64% sulfuric acid aqueous hydrolysis followed by high-pressure homogenization according to our previous report.[24−26] The liquid CNC suspension was freeze-dried to obtain dry CNC material for the current work. Semi-crystalline grade PLA (4032D, melting-flow index of 1.64 g·min^{-1}, number average molecular weight (M_n) of 4.5 × 10^4 g·mol^{-1})[27] was purchased from NatureWorks LLC (Minnetonka, MN, United States). It was dried in a vacuum oven at 60 °C for 24 h prior to use. MAH, dicumyl peroxide (DCP), *N*, *N*′- dimethylformamide (DMF), tetrahydrofuran (THF), and chloroform were purchased from Sigma-Aldrich Inc (St. Louis, MO, United States). All reagents were used without further purification. hASCs were kindly provided by Dr. Jeffery Gimble at the Pennington Biomedical Research Center of the Louisiana State University and used according to the LSU AgCenter IRB approved protocol HE 11-17.

Maleic Anhydride Grafted PLA (MPLA). The preparation process of MPLA was in accordance with the previously published procedure.[28] Briefly, MPLA was made by mixing PLA, MAH, and DCP (an initiator) in a Plasti-Corder torque rheometer (C.W. Brabender Instruments Inc., South Hackensack, NJ, United States) at 180 °C for 8 minutes at 60 rpm. The contents of MAH and DCP based on PLA weight were 3 and 0.3 wt %, respectively. To remove unreacted MAH and residual DCP, raw MPLA was completely dissolved in THF, and then was precipitated in excess of water and washed 10 times by water. The final MPLA powder was dried at 80 °C for 12 h to obtain pure MPLA. MPLA was characterized by Fourier-transform infrared spectra (FTIR, a Nicolet Magna-IR550 spectrophotometer, Thermo Scientific Inc., Madison, WI, United States) recorded in the region of 4000−400 cm^{-1} using KBr disks and gel permeation chromatography (GPC, Agilent PL-GPC 50, Santa Clara, CA, United States), as shown in Figures S1 and S2 in the Supporting Information (SI), respectively. FTIR data confirmed MAH grafting PLA (Scheme S1), as discussed in the SI. The weight average molecular weight (M_w), M_n, and the polydispersity index (PDI) were 5.87× 10^4 g·mol^{-1}, 2.7 × 10^4 g·mol^{-1}, and 2.17, respectively, indicating that the aforementioned process caused the decreased molecular weight from PLA to MPLA. During the modification process, the initiator induced free radicals on the PLA chains that mostly reacted with MAH to obtain MPLA. However, a few of these radicals might also react with oxygen in air to form peroxy radicals, which could subsequently form carbonyl groups and new chain-ends and finally cause the degradation of PLA.[29] Hence, MPLA had a smaller molecular weight than the original PLA.

Fabrication of Electrospun Fibrous Scaffolds. MPLA and freeze-dried CNC powder were added to a mixture of chloroform and DMF (volume ratio 8/2) with magnetic stirring for 30 min at 65 °C, followed by ultrasonic treatment for 30 min. The concentration of MPLA in the solution was fixed at 15 wt %. The loading levels of CNCs by the weight of MPLA were 1, 2, and 5 wt % because the dispersion of CNCs in electrospun PLA nanofibers weakens above the 5 wt % of CNC loading level.[20] The nomenclature of samples is designated as MPLA/CNC-*x*, where *x* (wt %) is the concentration of CNCs in relation to MPLA. The MPLA solutions and MPLA/CNC suspensions prepared were separately loaded in a 1-mL BD plastic syringe with a stainless steel needle (internal diameter 0.584 mm), and were then electrospun at a positive DC voltage of 15 kV and a flow rate of 1.5 mL·h^{-1}. A piece of grounded aluminum foil used as a collector was placed under the capillary needle tip with a distance of 20 cm. The obtained fibrous scaffolds were vacuum-dried at 80 °C for 24 h and then stored in a desiccator for further characterization.

Characterization of Electrospinning Solutions. Electrical conductivity of the prepared electrospinning solutions or suspensions was determined at room temperature using a Jenway model 4330 conductivity and PH meter (Bath, United Kingdom). The viscosity of the materials was measured by a AR2000 rheometer (TA Instruments, New Castle, DE, United States) at 25 °C and 10 s^{-1} of shear rate.

Morphological Observation and Composition Analysis. The surfaces of the electrospun scaffolds were sputter-coated with a thin layer of gold and their morphologies were evaluated by a field emission scanning electron microscopy (FESEM, a FEI Quanta 3D FEG dual beam SEM/FIB system, Hillsboro, OR, United States) at 5 kV. The fiber diameters were obtained from the analysis of SEM images using ImageJ 1.46 software (http://rsb.info.nih.gov/ij/), with 100 nanofibers randomly selected from each image. Selected composite suspensions were directly electrospun onto 400-mesh carbon-coated copper grids for 1 min to form thin fiber mats for further fiber evaluation using a transmission electron microscope (TEM) (JEOL 100CX, JEOL Inc., Peabody, MA, United States) at an accelerating voltage of 60 KV. Before observation, the sample was stained with a droplet of 2 % uranyl acetate for 60 seconds to enhance the contrast of images. To investigate the chemical composition, FTIR spectra of electrospun scaffolds were measured using a Bruker FTIR analyzer (Tensor-27, Bruker Optics, Billerica, MA, United States) with a Zn/Se crystal attenuated total reflectance (ATR) mode, in which each spectrum was acquired in an accumulation of 64 scans with a resolution of 4 cm^{-1} and a spectral range of 4000−600 cm^{-1}.

Thermal Properties. Thermogravimetric analysis (TGA) was conducted using a TA Q50 analyzer (TA Instruments, New Castle, DE, United States) to study thermal decomposition of electrospun

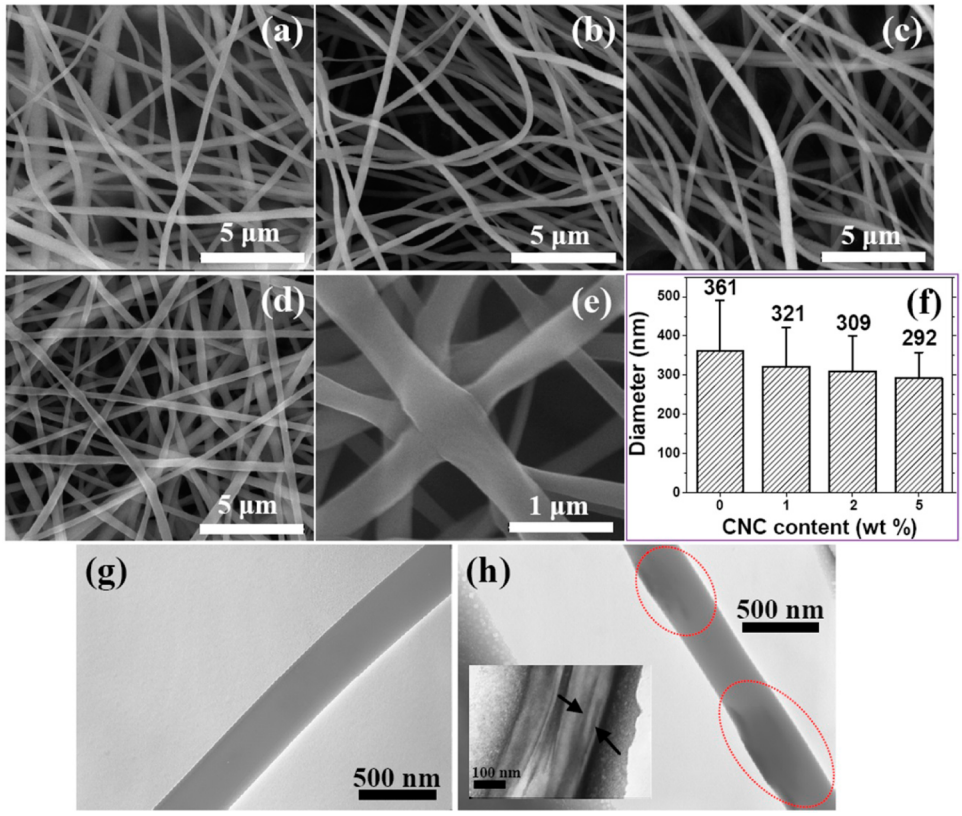

Figure 1. SEM micrographs of electrospun fibrous scaffolds: pure MPLA (a), MPLA/CNC-1(b), MPLA/CNC-2 (c), and MPLA/CNC-5 (d: 10 000×; e: 50 000×). (f) Relationship between CNC content and the diameter distribution for MPLA/CNC fibers. TEM micrographs of MPLA (g) and MPLA/CNC-5 with a magnified image illustrating the morphology of CNCs within fibers (h).

scaffolds. Samples of 5−10 mg were heated from room temperature to 600 °C at a rate of 10 °C·min^{-1} in a N_2 atmosphere. Differential scanning calorimetry (DSC) measurements of electrospun scaffolds were performed with a TA Q200 system. To remove any thermal history, samples of 5 ± 0.5 mg were heated to 200 °C at a heating rate of 30 °C·min^{-1}, and maintained at this temperature for 5 min followed by cooling to room temperature at a rate of 10 °C·min^{-1}. During subsequent test runs, the samples were reheated to 200 °C at a heating rate of 10 °C·min^{-1} and test data were collected.

The absolute enthalpy of fusion of MPLA in the composites was calculated as ΔH_p:

$$\Delta H_p = (\Delta H_m - \Delta H_{cc})/w \quad (1)$$

where ΔH_m (J/g) is the enthalpy of fusion of composites, ΔH_{cc} (J/g) is the enthalpy of cold crystallization of composites, and w is the weight fraction of MPLA in the composites. Because the absolute enthalpy of fusion of 100% crystalline MPLA (ΔH_{m0}) is unknown, the crystallization degree value (X_p) of MPLA could not be calculated using ΔH_p divided by ΔH_{m0}. However, ΔH_p, proportional to X_p, was used to show the change of X_p in this research.

To verify the reproducibility of the obtained TGA and DSC curves, two sample runs were performed under the same experimental conditions for each kind of scaffold. The approximate overlapping of two weight loss and heat flow curves from two separate test runs was considered as a reasonable agreement. Otherwise, another two runs were performed to determine which curve should be chosen.

Mechanical Properties. Tensile properties were measured using the TA AR2000 rheometer with a solid fixture at a tensile speed of 10 μm·s^{-1}. The tensile gauge length was fixed at 10 mm. Each sample group with the dimensions of 20 mm long, 3 mm wide, and 45 ± 8 μm thick was analyzed in triplicate. The stress and strain were calculated through the machine-recorded force and displacement based on the initial cross-section area and gauge length, respectively. The Young's modulus was calculated through a linear regression analysis using the initial linear portion of the stress−strain curves based on stress divided by strain of up to the 5% level.

In Vitro Degradation. The dried electrospun samples were cut into square pieces of 15 mm and weighed, and then were placed in sealed bottles containing 25 mL of phosphate buffer solution PBS (pH 7.3, Sigma-Aldrich). The bottles were immersed in a 37 °C water bath for 30 days. At target intervals, the samples were extracted and rinsed with DI water, dried in a vacuum oven, and re-weighed.

In Vitro Cell Viability. Circular samples of 10 mm diameter from the electrospun scaffolds were seeded with 60 mL of hASCs cell suspension at 1 × 10^5 cells/mL (n = 3) in a 12-well culture plate and cultured for 7 days in a humidified incubator (37 °C and 5% CO_2). Before cell seeding, all nanofibrous scaffolds were sterilized by UV irradiation. Cultures were maintained in Dulbecco's modified eagle growth medium consisting of nutrient mixture F-12 (DMEM/F-12, GIBCO, Invitrogen) supplemented with 10 % fetal bovine serum (FBS), 100 U of penicillin, 100 μg of steptomycin, and 0.25 μg of amphotericin (Fungizone). The AlamarBlue colorimetric assay (Invitrogen, Carlsbad, CA, United States) was used to assess the cell proliferation viability on the samples. On the seventh day, the scaffolds were removed from the culture, rinsed with PBS, and transferred to a fresh 12-well plate to avoid the possibility of measuring cells seeded on to the initial well bottom during the seeding process. The scaffolds were then incubated with 0.5 mL of 10% v/v AlamarBlue in a stromal medium solution for 4 h. Then a 100-mL sample of the mixture was transferred to a 96-well plate. The fluorescence of AlamarBlue was measured using a Wallac VICTOR2 V 1420-040 multilabel counter at excitation and emission wavelengths of 523 and 595 nm, respectively. Scaffolds with no cells were used as negative control and the fluorescence of each was subtracted from its respective scaffold with hASC. Live cells were also seeded on empty wells at the same density and were used as the positive control. All experiments were conducted in triplicate. One-way analysis of variance (ANOVA) was performed to determine statistical significance of the data. Differences were

Table 1. Viscosities and Conductivity of Electrospinning MPLA Solutions and MPLA/CNC Suspensions, Diameter of MPLA and MPLA/CNC Fibers, and Molecular Weight of MPLA and MPLA/CNC Scaffolds before and after In Vitro Degradation

sample	μ (mPa·s)	σ (μS·cm^{-1})	diameter (nm)	M_n (10^4 g·mol^{-1})	$M_n'^{a}$ (10^4 g·mol^{-1})
MPLA	12.0	1.21	361 ± 130	2.71	1.87
MPLA/CNC-1	12.2	1.25	321 ± 101		
MPLA/CNC-2	12.5	1.27	309 ± 91		
MPLA/CNC-5	13.1	1.30	292 ± 66	2.75	2.18
PLA/CNC-5[20]	16.0	0.67	642 ± 71	4.56	

[a] M_n' is the average molecular weight of MPLA with 30 days of in vitro degradation.

considered significant at $P < 0.05$. Additionally, the cytotoxic effects of the nanofibrous scaffolds on hASCs were also evaluated by a fluorescence scanning confocal microscope. Live/dead staining was performed on the seeded scaffolds for visualization of cellular viability by using LIVE/DEAD Viability/Cytotoxicity Kit (Invitrogen) according to the manufacturer's instructions.

RESULTS AND DISCUSSION

Microstructure and Chemical Analysis of Nanofibrous Scaffolds. SEM photographs of electrospun MPLA and MPLA/CNC fibrous composites are shown in Figure 1a–e. Figure 1f and Table 1 show the calculated average diameters and diameter deviations of the electrospun fibers. All fibers produced were homogeneous without visible beads, and exhibited decreased average diameters and polydispersity with increased CNC contents, which is similar with the morphologic changes observed in the electrospun PLA/CNC and PEO/CNC nanocomposite fibers in our previous report.[20,30] The average diameters of pure MPLA and MPLA/CNC-5 fibers were 361 and 292 nm, respectively, with a more uniform distribution of diameter for MPLA/CNC-5 fibers compared with MPLA fibers.

It is well known that the change of diameter of electrospun nanofibers incorporated by nanoparticles is mostly attributed to the charge density and visco-elastic behavior of electrospinning solutions when using the same polymer concentration and solvent for the electrospinning solutions. The electrical conductivity (σ, μS·cm^{-1}) and viscosity (μ, mPa·s) of the electrospinning MPLA solutions and MPLA-CNC suspensions were measured, and the results are shown in Table 1. The values of μ and σ were 12.0 mPa·s and 1.21 μS·cm^{-1} for MPLA, and 13.1 mPa·s and 1.30 μS·cm^{-1} for MPLA/CNC-5. Viscosities of the electrospinning MPLA solutions filled with CNCs increased with the increase of CNC contents. Many previous studies have shown this observation, which could be attributed to the formed network structure of CNCs within the polymer solutions.[20,31] The increased conductivity of MPLA/CNC suspensions was because of the negatively charged CNCs from the sulfate ester groups on its surface produced during the process of sulfuric acid hydrolysis.[32] In general, the effect of the electrical conductivity is opposite the effect of viscosity in controlling the diameter of the electrospun fibers (i.e., the increase in electrical conductivity of the suspension favors the formation of smaller fibers while the increase in viscosity favors forming bigger fibers). Hence, the decrease in the average diameter from MPLA to MPLA/CNC-5 fibers indicates that conductivity effects were more obvious than those of viscosity. This behavior might be attributed to increased electrostatic forces becoming dominant for non-conductive polymers (PLA or MPLA), inducing more extensive jets to be elongated during the whipping instability.[33,34] Increased viscosity tended to result in thicker electrospun nanofibers, which, however, could also make fibers more uniform.[17] Hence, the decrease in diameter polydispersity of MPLA/CNC nanofibers with increased CNC contents (Figure 1f) could be attributed to the increased viscosity. Figure 1e shows bonds between homogeneous MPLA/CNC-5 nanofibers by a higher magnification. This dense inter-fiber bonding could result in improved mechanical properties for scaffolds.

In addition, it has been reported that the electrospun PLA/CNC-5 fibers had an average diameter of 642 nm,[20] indicating the obvious decrease in electrospun fiber diameter from PLA to MPLA-based bio-composites at the same CNC content. Because the viscosity and conductivity of suspensions at the 5 wt % of CNC loading level were 16.0 mPa·s and 0.67 μS·cm^{-1} for PLA and 13.1 mPa·s and 1.30 μS·cm^{-1} for MPLA (Table 1), both effects (i.e., the decreased viscosity and the increased electrical conductivity in the electrospinning nanocomposite suspensions from PLA/CNC to MPLA/CNC) favored this change. The decreased μ was the result of decreased molecular weight of MPLA because of the thermal degradation during the modification process, as depicted in GPC result of Table 1 (i.e., M_n of PLA and MPLA being 4.56×10^4 and 2.71×10^4 g·mol^{-1}, respectively). The substantial increase of suspension conductivity from PLA to MPLA was attributed to the greater polarity of MAH grafted PLA.

Moreover, unlike PLA/CNC fibers, the surface of MPLA/CNC fibers was smooth and dense without the existence of visual pores. Figure 1g and h show the TEM micrographs of the MPLA and MPLA/CNC-5 fibers, respectively. It can be observed that MPLA and MPLA/CNC-5 fibers had diameters of approximately 360 and 290 nm, respectively, which was consistent with the results of the SEM observation. It can also be seen that some black rods, attributed to CNCs particles as well as some CNC aggregates, were visible, as indicated by red cycle in Figure 1h, confirming the presence of CNCs in MPLA/CNC nanocomposite fibers. At higher magnifications, the rod-shaped CNCs, as highlighted by the arrows in Figure 1h insert, were highly aligned along the nanofiber long-axis and had a diameter of about 10 nm, which agreed well with the diameters of single cellulose nanocrystal. Therefore, it is concluded that well-dispersed CNCs, not only in water-soluble polymer matrix[25] but also in water-insoluble matrix, could obtain a high degree of orientation through a high-voltage electric field.

To analyze the chemical composition of the electrospun fibrous scaffolds, FTIR spectra of fibrous MPLA and MPLA/CNC-5 scaffolds are shown in Figure 2. Compared with MPLA scaffolds, the spectrum of MPLA/CNC-5 had additional three characteristic absorbance peaks at 3335 (ranging from 3450 to 3100 cm^{-1}), 2970, and 1053 cm^{-1}, which could be assigned to the hydrogen-bond O–H stretching, methyl and methylene C–H stretching, and C–O at C_6 stretching vibrations in CNCs,[21] respectively. This result further indicated that CNCs were indeed present on the electrospun fibers and were not

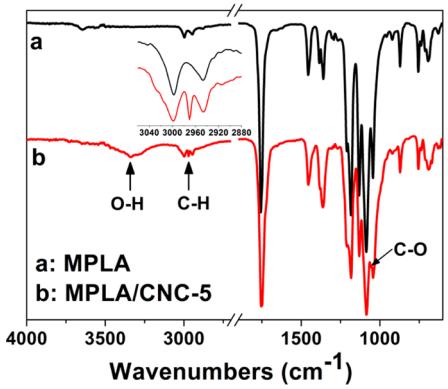

Figure 2. FTIR spectra of MPLA (a) and MPLA/CNC-5 (b) fibrous scaffolds.

selectively excluded during the electrospinning process. In addition, end O−H stretching peak of MPLA at ca. 3700−3450 cm^{-1} in the MPLA (Figure 2a) shifted to ca. 3500−3100 cm^{-1} in MPLA/CNC-5 composites (Figure 2b) and overlaid with O−H peak of CNCs. This is likely because the strong hydrogen bonds between CNCs and MPLA chains weakened the intermolecular and intra-molecular hydrogen bonds of MPLA chains themselves.

Thermal and Mechanical Properties. Thermal properties of pure MPLA and MPLA/CNC fibrous scaffolds are summarized in Table 2 based on TG/DTG and DSC curves

Table 2. Summary of TGA and DSC Data of Electrospun MPLA and MPLA/CNC Fibrous Scaffolds

sample	T_{max} (°C)	CY[a] (wt %)	T_g (°C)	T_m (°C)	ΔH_{cc} (J/g)	ΔH_m (J/g)	ΔH_p[b] (J/g)
MPLA	348.0	2.3	60.0	167.9	22.5	44.5	22.0
MPLA/CNC-1	347.7	12.7	59.3	167.6	18.7	43.0	24.6
MPLA/CNC-2	348.6	13.4	60.0	168.1	18.2	43.6	25.9
MPLA/CNC-5	353.6	23.3	60.5	168.3	20.0	44.9	26.2
PLA/CNC-5[20]	357.5	6.8	62.5	166.7[c]	24.0	30.3	6.6

[a]CY is char yield. [b]ΔH_p is the enthalpy of fusion of MPLA or PLA in the composites. [c]The value is the main peak, and PLA/CNC-5 had the other small melt peak at about 165 °C.

(Figure 3). The maximum thermal degradation temperatures (T_{max}) of MPLA and MPLA/CNC-5 were 348.0 and 353.6 °C, respectively, indicating that the incorporation of CNCs improved the heat resistance of composites. Although T_{max} of CNCs was below 310 °C, its char yield was up to 39 %.[25] Before the thermal decomposition point of MPLA, char is produced from CNCs. The char formation inhibited the thermal conductivity,[35] and then increased T_{max} of MPLA/CNC nanocomposite scaffolds. From Table 2, it is also seen that the char yield of MPLA/CNC composites obviously increased with increased CNC content, further indicating the role of CNCs in promoting the thermal resistance of composites.

As shown in Table 2, with increased CNC contents, the glass transition temperature (T_g) and the melting temperature (T_m) of MPLA/CNC composite scaffolds had no obvious change. However, unlike PLA/CNC composite scaffolds with the 5 wt % of CNC loading level, which had two melt peaks,[20] MPLA/CNC-5 composite scaffolds just had one peak. This indicates that the grafting MAH effectively improved the interface adhesion between polymer matrix and CNCs. In this way, MPLA was used as a compatibilizing agent in the biocomposites consisting of PLA and natural carbohydrate polymers.[36,37] Table 2 also shows the absolute enthalpy of fusion of MPLA in the composites ΔH_p. It can be seen that ΔH_p of MPLA gradually increased with increased CNC content, indicating that the presence of CNCs improved the crystallization of MPLA molecular chains likely because CNCs acted as a nucleating agent.

The mechanical properties of tensile strength and elasticity are essential for simple implantation and long-term success of a tissue-engineered scaffold. Figure 4 shows typical tensile stress−strain curves of pure MPLA and MPLA/CNC fibrous scaffolds. With the increased content of CNC, the curves were shifted toward higher values of stress, indicating the reinforcement of fibrous scaffolds. To further describe the tensile properties of the electrospun materials, the corresponding values of the maximum tensile stress (σ_{max}), Young's modulus (E), and the elongation at break (ε_b) are summarized in Table 3. The tensile strength (i.e., σ_{max}) increased progressively with the addition of CNCs, whereas ε_b decreased markedly, making scaffolds much stronger and more resistant to deformation. This is expected because the addition of CNCs into MPLA nanofibers caused the increased crystallinity (as depicted in Table 2) and reduced the loading force on MPLA through the stress transfer from MPLA to CNCs based on their strong physical crosslinking or interaction.[30] In terms of E, a similar increase with increased CNC content is observed, indicating the enhanced interaction among nanocomposite fibers likely attributed to the formation of more uniform and finer fibers induced by the addition of CNCs (as depicted in Figure 1). It is also noted that σ_{max} values from MPLA/CNC-1 to MPLA/CNC-2 scaffolds only had a slight increase. Although mechanical properties of electrospun scaffolds are controlled by many factors including composition and structure of individual fibers, and the interaction among fibers, our previous research indicated that the strength of electrospun scaffolds depended more on the composition of individual fibers, (e.g., the effect of incorporated CNCs).[20] Within an individual nanocomposite fiber, the dispersion, orientation, and interfacial adhesion of nanoparticles within polymer matrix had the most reinforcement effects associated with a mechanical percolation.[38] According to Favier's study on three-dimensional percolating structures using cellulose fibers to reinforce latex matrix,[39] the percolation threshold of CNC reinforcing MPLA was estimated at 4.4 wt % based on the aspect ratio of the used CNCs. Because there were no direct links among CNCs below the percolation threshold, the scaffold's mechanical properties might be only slightly improved below the 4.4 wt % of CNC loading level. The fibrous MPLA/CNC nanocomposite scaffolds with the 5 wt % CNC loading level had the best strength and modulus (i.e., 10.8 and 135.1 MPa, respectively) among CNC contents used, and increased by approximate 6 and 16 fold in tensile strength and modulus, respectively, compared with the electrospun fibrous MPLA scaffolds. In contrast, the tensile strength and modulus of fibrous PLA/CNC-5 nanocomposite scaffolds were reported in our previous work to be 6.3 and 125.6 MPa, respectively.[20] The obvious increase in mechanical properties (especially in the strength, nearly 1-fold) from PLA/CNC to MPLA/CNC composite

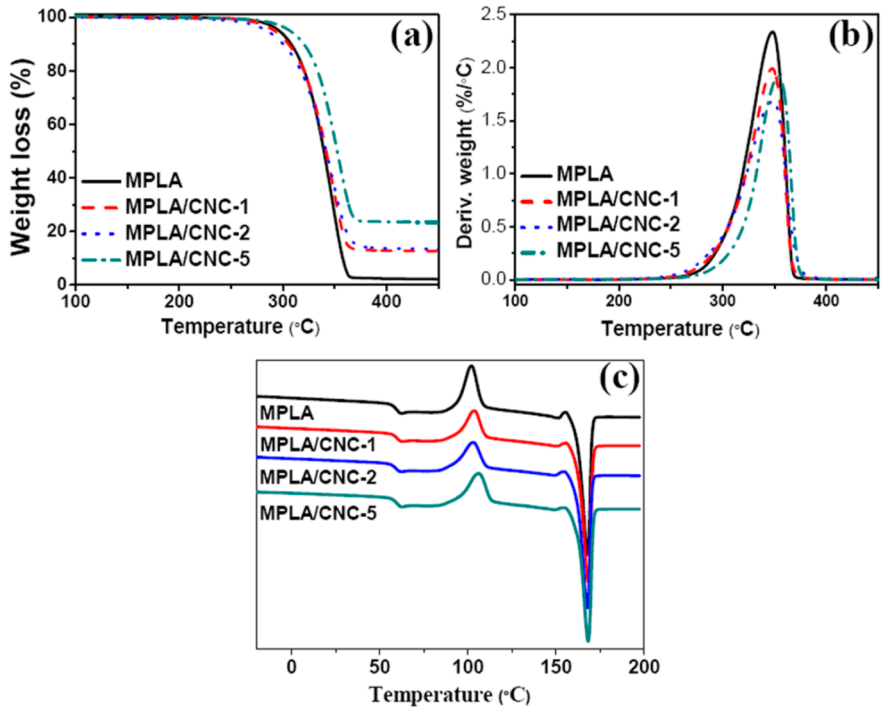

Figure 3. TG (a), DTG (b), and DSC (c) curves of electrospun pure MPLA and MPLA/CNC fibrous scaffolds.

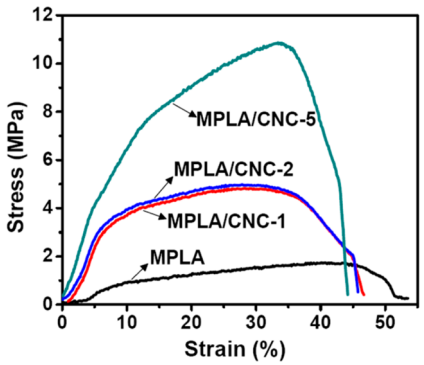

Figure 4. Typical tensile stress−strain curves of electrospun MPLA and MPLA/CNC fibrous scaffolds.

Table 3. Tensile prOperties of Electrospun MPLA and MPLA/CNC Fibrous Scaffolds

testing sample	σ_{max} (MPa)	E (MPa)	ε_b (%)
MPLA	1.6 ± 0.4	7.8 ± 3.1	51.8 ± 3.8
MPLA/CNC-1	4.8 ± 0.8	77.2 ± 7.8	46.9 ± 4.3
MPLA/CNC-2	4.9 ± 1.0	87.4 ± 8.0	45.8 ± 4.7
MPLA/CNC-5	10.8 ± 1.7	135.1 ± 10.4	44.0 ± 5.1
PLA/CNC-5[20]	6.3 ± 1.2	125.6 ± 9.9	68.4 ± 14.2

scaffolds at the same CNC content is attributed to the polar of MAH improving the adhesive between polymer matrix and CNCs.

Therefore, MPLA/CNC-5 composite scaffold was identified as the optimum system based on mechanical and thermal properties for comparison below.

In Vitro Degradation. In vitro degradation of scaffolds in the PBS medium was evaluated by mass loss in 30 days. Figure 5a shows the mass loss of MPLA and MPLA/CNC-5 scaffolds with the degradation time. As shown in Figure 5a, both scaffolds exhibited a high mass loss rate within the first 6 days

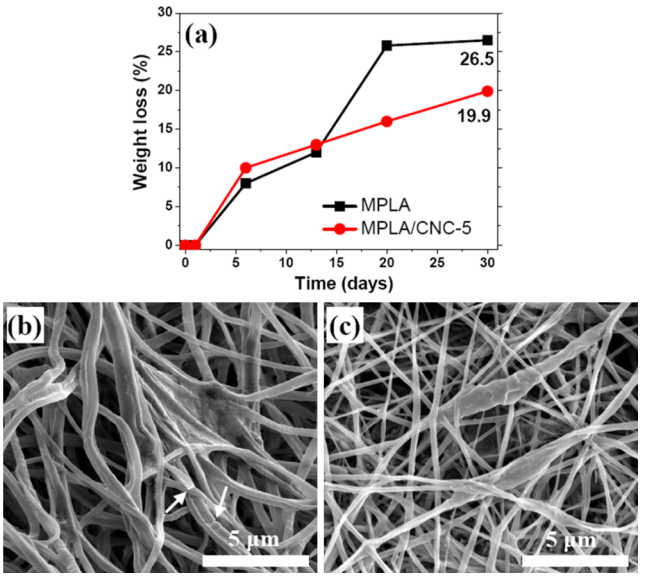

Figure 5. Weight loss of electrospun pure MPLA and MPLA/CNC-5 scaffolds as a function of degradation time (a), and SEM pictures of in vitro degradation for pure MPLA (b) and MPLA/CNC-5 scaffolds (c) after one month.

(except for the first day), which is likely due to the fast penetration of PBS into the pore structure of the scaffolds resulting in the simple hydrolysis of the ester backbone on the easily accessible surfaces of nanofibers. It is worth noting that the degradation rate of MPLA/CNC-5 in this stage was higher than that of MPLA likely because of the larger surface area of MPLA/CNC-5 scaffold resulting from its lower fiber diameter (Figure 1). After this period, the mass loss of MPLA/CNC-5 scaffold accelerated gradually, while the weight loss of pure MPLA scaffolds had a sharp acceleration at the 13th day of degradation, suggesting severe degradation because of the

dx.doi.org/10.1021/am4005072 | ACS Appl. Mater. Interfaces 2013, 5, 3847−3854

formation of surface defects and the rupture of nanofibers (discussed later in SEM morphological analysis). At the 30th day, the mass loss of MPLA and MPLA/CNC-5 scaffolds reached 26.5 and 19.9 wt %, respectively, which is in agreement with the change of their molecular weight after in vitro degradation of 30 days (1.87×10^4 and 2.18×10^4 g·mol^{-1} for MPLA and MPLA/CNC-5, respectively, shown in Table 1) and similar to the hydrolytic degradation results of poly(D,L-lactide)/CNCs in PBS.[40] This suggests that the addition of CNCs reduced in vitro degradation rate of MPLA/CNC scaffolds in PBS by increasing the crystallinity of MPLA (as stated in DSC results above) and inhibiting the diffusion of water in the polymer matrix,[18] even though the addition CNCs resulted in a higher total surface area for MPLA/CNC scaffolds. In contrast, PLA/CNC-5 scaffolds, unlike MPLA/CNC-5 scaffolds, showed a rapid degradation rate and a weight loss of approximately 40% in one month.[20] The phenomenon is expected to be a result of the improved adhesion between CNC and MAH modified PLA, which inhibited the formation of pores on the surface of electrospun nanofibers (occurred at PLA/CNC nanofibers due to the phase separation between immiscible PLA and CNCs), as aforementioned SEM observation in Figure 1.

Figure 5b and c illustrate the morphologies of the pure MPLA and MPLA/CNC-5 scaffolds after the exposure to PBS for one month, respectively. For degraded MPLA scaffolds (Figure 5b) compared with original MPLA scaffolds (Figure 1a), a large number of nanofibers swelled and degraded while restructuring to form an amorphous mass.[41] Additionally several nanofibers can be seen in the process of dissolution, as indicated by the inserted arrows. No significant morphological change in degraded MPLA/CNC-5 scaffolds in comparison to original counterparts (Figure 1d) was observed other than some merged fibers, which supported the prolonging degradation ability in nanocomposite scaffolds by the incorporation of CNCs, as shown in Figure 5a.

Cytocompatibility. The hASCs used were cultured on nanofibrous scaffolds composed of PLA/CNC and MPLA/CNC composites with a CNC content of 5 wt % to assess the basic cytocompatibility of these materials and to evaluate their potential for use in bone tissue engineering applications. LIVE/DEAD viability/cytotoxicity kit (Invitrogen) (a fluorescent live/dead microscopy stain) and AlamarBlue assay (a colorimetric/fluorometric metabolic indicator) were used for the qualitative and quantitative viability analyses of hASCs on nanofibrous scaffolds, respectively, as shown in Figure 6. Figure 6a–d show fluorescence images of hASCs cultured on PLA/CNC and MPLA/CNC nanofibrous scaffolds. Live cells (stained green) cultured on the MPLA/CNC-5 nanofibrous scaffolds were obviously more numerous than those on the PLA/CNC-5 nanofibrous scaffolds, and showed a spindle-like morphology. This is attributed to the formation of nanofibrous morphology in MPLA/CNC scaffolds resulting from the greatly decreased diameter of nanofibers, promoting cell–matrix interactions by providing more binding sites for cell adhesion and proliferation.[42−44] Additionally, slower degradation rate of MPLA/CNC scaffolds may have resulted in improved cell adhesion and proliferation. Very few dead cells (stained red) were also detected on MPLA/CNC-5 nanofibrous scaffolds, indicating the reduced cytotoxicity during hASCs cultivation. Results of AlamarBlue proliferation viability assay (Figure 6e) show that the percentage of live cells was 85.4, 100.0, 78.7, and 92.3 % for PLA, MPLA, PLA/CNC-5, and MPLA/CNC-5

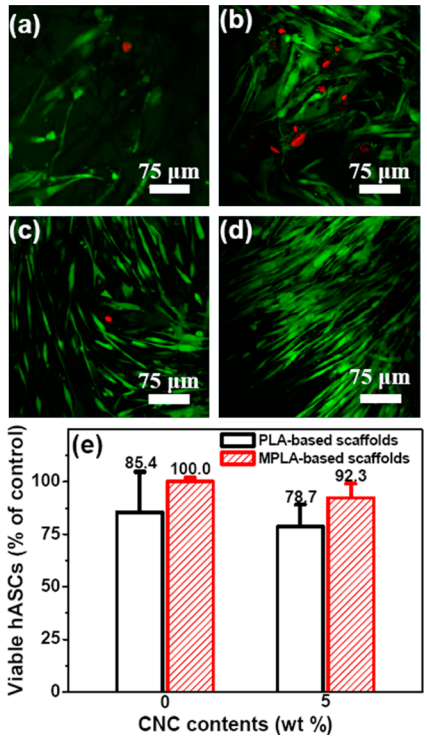

Figure 6. Responsed of hASCss to PLA/CNC and MPLA/CNC nanofibrous scaffolds after 7 days of culture. Fluorescence micrographs of stained cells consisting of live (green) and dead (red) cells for PLA (a), PLA/CNC-5 (b), MPLA (c), and MPLA/CNC-5 (d) scaffolds, scale bar represents 75 μm; proliferation viability of cells (e).

scaffolds, respectively. The differences of those values were not significant ($P > 0.05$ from ANOVA analysis). This means that the incorporation of CNCs into scaffolds did not have a significant cytotoxic effect on hASCs proliferation within 7 days because the concentration of CNCs (approximately 50 μg·mL^{-1} by the volume of cell medium) was too low to cause the cell death. Recently, it was reported that in vitro exposure of cotton cellulose nanofibers (below 100 μg·mL^{-1} of concentration) was not cytotoxic to bovine fibroblasts.[45] Hence, MPLA/CNC-5 composite scaffolds were capable of supporting cell proliferation, and possess good cytocompatibility.

CONCLUSIONS

Electrospun MPLA/CNC bio-nanocomposite scaffolds were successfully prepared using MAH grafted PLA as matrix for the enhanced interaction between CNCs and matrix. Morphological investigation indicated that MPLA/CNC nanofibers became more uniform and finer with increased CNC contents. The thermal and tensile test results revealed that the addition of CNCs effectively improved the thermal stability and mechanical properties of MPLA/CNC scaffolds. MPLA/CNC-5 scaffolds showed not only superior tensile strength (more than 10 MPa), but also excellent stability during in vitro degradation compared to the pure MPLA and PLA/CNC-5 counterpart scaffolds. This was ascribed to the effective improvement of interfacial adhesion between CNCs and polymer matrix through MAH grafting on PLA, which inhibited their phase separation and facilitated the efficient stress transfer from MPLA to CNCs. Moreover, MPLA/CNC fibrous scaffolds were non-toxic to hASCs and capable of supporting cell proliferation. This study

for the first time demonstrates that the improved interaction from CNCs and MAH grafted PLA can promote the formation of ECM nanofibrous microstructure, enhance the mechanical properties, and induce the biodegradable and cytocompatible properties for MPLA/CNC scaffolds. Therefore, the electrospun MPLA/CNC bio-nanocomposite nanofibrous scaffolds fabricated fulfill many requirements for effective implantation and could be potentially suitable in the bone tissue engineering field, which may greatly contribute to the development of CNCs as advanced function materials.

■ ASSOCIATED CONTENT

Supporting Information

FTIR spectra of PLA and MPLA, a scheme of chemical reaction between PLA and MAH for preparing MPLA, and GPC curves of MPLA. This material is available free of charge via the Internet at http://pubs.acs.org.

■ AUTHOR INFORMATION

Corresponding Author

*E-mail: wuqing@lsu.edu. Tel.: +1 225 578 8369. Fax: +1 225 578 4251.

Notes

The authors declare no competing financial interest.

■ ACKNOWLEDGMENTS

This work is financially supported by financial support from the Louisiana Board of Regents (LEQSF-EPS(2013)-PFUND-318) and the National Key Technology R&D Program of China (2012BAD32B01). L.T. and D.H. thank Dr. Jeffery Gimble for providing hASCs.

■ REFERENCES

(1) Samir, M. A. S. A.; Alloin, F.; Dufresne, A. *Biomacromolecules* **2005**, *6*, 612−626.
(2) Habibi, Y.; Lucia, L. A.; Rojas, O. J. *Chem. Rev.* **2010**, *110*, 3479−3500.
(3) Moon, R. J.; Martini, A.; Nairn, J.; Simonsen, J.; Youngblood, J. *Chem. Soc. Rev.* **2011**, *40*, 3941−3994.
(4) Eichhorn, S. J. *Soft Matter* **2011**, *7*, 303−315.
(5) Habibi, Y.; Heim, T.; Douillard, R. *J. Polym. Sci., Part B: Polym. Phys.* **2008**, *46*, 1430−1436.
(6) Olsson, R. T.; Kraemer, R. H.; Lopez-Rubio, A.; Torres-Giner, S.; Ocio, M. J.; Lagaron, J. M. *Macromolecules* **2010**, *43*, 4201−4209.
(7) Dong, H.; Strawhecker, K. E.; Snyder, J. F.; Orlicki, J. A.; Reiner, R. S.; Rudie, A. W. *Carbohydr. Polym.* **2012**, *87*, 2488−2495.
(8) Gupta, B.; Revagade, N.; Hilborn, J. *Prog. Polym. Sci.* **2007**, *32*, 455−482.
(9) Rasal, R. M.; Janorkar, A. V.; Hirt, D. E. *Prog. Polym. Sci.* **2010**, *35*, 338−356.
(10) Wei, G. B.; Ma, P. X. *Biomaterials* **2004**, *25*, 4749−4757.
(11) Hutmacher, D. W. *Biomaterials* **2000**, *21*, 2529−2543.
(12) Xiong, Z.; Yan, Y. N.; Zhang, R. J.; Sun, L. *Scr. Mater.* **2001**, *45*, 773−779.
(13) Kim, K.; Yu, M.; Zong, X. H.; Chiu, J.; Fang, D. F.; Seo, Y. S.; Hsiao, B. S.; Chu, B.; Hadjiargyrou, M. *Biomaterials* **2003**, *24*, 4977−4985.
(14) Zhou, C. J.; Wu, Q. J. Recent Development in Applications of Cellulose Nanocrystals for Advanced Polymer-Based Nanocomposites by Novel Fabrication Strategies. In *Nanocrystals - Synthesis, Characterization and Applications*; Neralla, S., Ed.; InTech, 2012; pp 103−120.
(15) Sui, G.; Yang, X. P.; Mei, F.; Hu, X. Y.; Chen, G. Q.; Deng, X. L.; Ryu, S. *J. Biomed. Mater. Res., Part A* **2007**, *82A*, 445−454.
(16) Noh, K. T.; Lee, H. Y.; Shin, U. S.; Kim, H. W. *Mater. Lett.* **2010**, *64*, 802−805.
(17) Xiang, C. H.; Joo, Y. L.; Frey, M. W. *J. Biobased Mater. Bioenergy* **2009**, *3*, 147−155.
(18) Ramirez, M. A. *Cellulose Nanocrystals Reinforced Electrospun Poly(lactic acid) Fibers as Potential Scaffold for Bone Tissue Engineering*. M.S. Thesis, North Carolina State University, Raleigh, NC, 2010.
(19) Liu, D. Y.; Yuan, X. W.; Bhattacharyya, D. *J. Mater. Sci.* **2012**, *47*, 3159−3165.
(20) Shi, Q. F.; Zhou, C. J.; Yue, Y. Y.; Guo, W. H.; Wu, Y. Q.; Wu, Q. L. *Carbohydr. Polym.* **2012**, *90*, 301−308.
(21) Zoppe, J. O.; Peresin, M. S.; Habibi, Y.; Venditti, R. A.; Rojas, O. J. *ACS Appl. Mater. Interfaces* **2009**, *1*, 1996−2004.
(22) Zhang, J. F.; Sun, X. Z. *Biomacromolecules* **2004**, *5*, 1446−1451.
(23) Zanetti, A. S.; Sabliov, C.; Gimble, J. M.; Hayes, D. J. *J. Biomed. Mater. Res., Part B* **2013**, *101B*, 187−199.
(24) Zhou, C. J.; Wu, Q. L.; Yue, Y. Y.; Zhang, Q. G. *J. Colloid Interface Sci.* **2011**, *353*, 116−123.
(25) Yue, Y. Y.; Zhou, C. J.; French, A. D.; Xia, G.; Han, G. P.; Wang, Q. W.; Wu, Q. L. *Cellulose* **2012**, *19*, 1173−1187.
(26) Zhou, C. J.; Wu, Q. L.; Zhang, Q. G. *Colloid Polym. Sci.* **2011**, *289*, 247−255.
(27) Shi, Q. F.; Mou, H. Y.; Gao, L.; Yang, J.; Guo, W. H. *J. Polym. Environ.* **2010**, *18*, 567−575.
(28) Avella, M.; Bogoeva-Gaceva, G.; Bularovska, A.; Errico, M. E.; Gentile, G.; Grozdanov, A. *J. Appl. Polym. Sci.* **2008**, *108*, 3542−3551.
(29) Babanalbandi, A.; Hill, D. J. T.; Hunter, D. S.; Kettle, L. *Polym. Int.* **1999**, *48*, 980−984.
(30) Zhou, C. J.; Chu, R.; Wu, R.; Wu, Q. L. *Biomacromolecules* **2011**, *12*, 2617−2625.
(31) Ago, M.; Okajima, K.; Jakes, J. E.; Park, S.; Rojas, O. J. *Biomacromolecules* **2012**, *13*, 918−926.
(32) Zhou, C. J.; Wang, Q. W.; Wu, Q. L. *Carbohydr. Polym.* **2012**, *87*, 1779−1786.
(33) Reneker, D. H.; Yarin, A. L. *Polymer* **2008**, *49*, 2387−2425.
(34) Baji, A.; Mai, Y. W.; Wong, S. C.; Abtahi, M.; Chen, P. *Compos. Sci. Technol.* **2010**, *70*, 703−718.
(35) Liepins, R.; Pearce, E. M. *Environ. Health Perspect.* **1976**, *17*, 55−63.
(36) Oksman, K.; Mathew, A. P.; Bondeson, D.; Kvien, I. *Compos. Sci. Technol.* **2006**, *66*, 2776−2784.
(37) Huneault, M. A.; Li, H. B. *Polymer* **2007**, *48*, 270−280.
(38) Zhou, C. J.; Wang, S. F.; Zhang, Y.; Zhuang, Q. X.; Han, Z. W. *Polymer* **2008**, *49*, 2520−2530.
(39) Favier, V.; Dendievel, R.; Canova, G.; Cavaille, J. Y.; Gilormini, P. *Acta Mater.* **1997**, *45*, 1557−1565.
(40) de Paula, E. L.; Mano, V.; Pereira, F. V. *Polym. Degrad. Stab.* **2011**, *96*, 1631−1638.
(41) You, Y.; Min, B. M.; Lee, S. J.; Lee, T. S.; Park, W. H. *J. Appl. Polym. Sci.* **2005**, *95*, 193−200.
(42) Bhattarai, N.; Edmondson, D.; Veiseh, O.; Matsen, F. A.; Zhang, M. Q. *Biomaterials* **2005**, *26*, 6176−6184.
(43) Lee, S. J.; Oh, S. H.; Liu, J.; Soker, S.; Atala, A.; Yoo, J. J. *Biomaterials* **2008**, *29*, 1422−1430.
(44) Cooper, A.; Jana, S.; Bhattarai, N.; Zhang, M. Q. *J. Mater. Chem.* **2010**, *20*, 8904−8911.
(45) Pereira, M. M.; Raposo, N. R. B.; Brayner, R.; Teixeira, E. M.; Oliveira, V.; Quintao, C. C. R.; Camargo, L. S. A.; Mattoso, L. H. C.; Brandao, H. M. *Nanotechnology* **2013**, *24*, 075103.